frontiers | Frontiers in Energy Research

TYPE Original Research
PUBLISHED 16 November 2023
DOI 10.3389/fenrg.2023.1283079

OPEN ACCESS

EDITED BY
Peng Tan,
CNPC Engineering Technology R&D Company Limited, China

REVIEWED BY
Li Qingmiao,
Chengdu University of Technology, China
Shixiang Tian,
Guizhou University, China

*CORRESPONDENCE
Zhiheng Cheng,
zh_cheng_2021@126.com
Chunyuan Li,
lcy6055@163.com

RECEIVED 25 August 2023
ACCEPTED 30 October 2023
PUBLISHED 16 November 2023

CITATION
Xuan Z, Cheng Z, Li C, Fan C, Qin H, Li W, Guo K, Chen H, Xie Y and Yang L (2023), Energy evolution mechanism during rockburst development in structures of surrounding rocks of deep rockburst-prone roadways in coal mines. *Front. Energy Res.* 11:1283079. doi: 10.3389/fenrg.2023.1283079

Energy evolution mechanism during rockburst development in structures of surrounding rocks of deep rockburst-prone roadways in coal mines

Zhongtang Xuan[1,2,3], Zhiheng Cheng[4]*, Chunyuan Li[5]*, Chaojun Fan[6], Hongyan Qin[7], Wenchen Li[4], Kai Guo[8], Haoyi Chen[8], Yifei Xie[4] and Likai Yang[4]

[1]Chinese Institute of Coal Science, Beijing, China, [2]China University of Mining and Technology (Beijing), Beijing, China, [3]China Coal Research Institute, Beijing, China, [4]School of Mining Safety, North China Institute of Science and Technology, Beijing, China, [5]Deep Mining and Rockburst Prevention Institute, China Institute of Coal Science, Beijing, China, [6]College of Mining, Liaoning Technical University, Fuxin, China, [7]School of Safety Engineering, North China Institute of Science and Technology, Beijing, China, [8]School of Civil and Resource Engineering, University of Science and Technology Beijing, Beijing, China

Influenced by the deep high-stress environment, geological structures, and mining disturbance in coal mines, the frequency of rockburst disasters in roadways is increasing. This research analyzed energy evolution characteristics during rockburst development in the elastic bearing zone and energy conversion in the plastic failure zone. The critical energy criteria for structural instability of roadway surrounding rocks were deduced. Numerical software was also applied to simulate the energy evolution during rockburst development in surrounding rocks of rockburst-prone roadways under conditions of different mining depths and coal pillar widths. The occurrence mechanism of rockburst deep in coal mines was analyzed from the perspective of energy in structures of deep roadway surrounding rock in coal mines. The research results show that the critical energy criteria are closely related to the elastic strain energy stored in deep roadway surrounding rocks and the energy absorbed by support systems. The impact energy in roadways is directly proportional to the square of the stress concentration factor k. Moreover, as the mining depth increases, the location of the peak point of maximum energy density gradually shifts to coal ahead of the working face. The larger the mining depth is, the more significantly the energy density is influenced by advanced abutment pressure of the working face and the wider the affected area is. With the increment of the coal pillar width, the distance from the peak point of energy density to the roadway boundary enlarges abruptly at first and then slowly, and the critical coal pillar width for gentle change in the distance is 30 m. Changes in the peak elastic energy density in coal pillars with the coal pillar width can be divided into four stages: the slow increase stage, abrupt increase stage, abrupt decrease stage, and slow decrease stage. The elastic energy density is distributed asymmetrically in deep roadway surrounding rocks in coal mines. Under the action of structures of roadway surrounding rocks, energy evolution in these structures differs greatly during rockburst development

under conditions of different coal pillar widths. This research provides an important theoretical basis for the support of rockburst-prone roadways during deep coal mining.

KEYWORDS

energy evolution mechanism, rockburst, deep coal mines, rockburst-prone roadways, structures of surrounding rocks

1 Introduction

Coal is the main energy source that supports the economic development in China (Wu et al., 2022; Sun D. L. et al., 2023; Su et al., 2023). In the recent decade, the raw coal yield in China has always been high (Tan P. et al., 2023; Zhang et al., 2023a; Wu et al., 2023), with huge annual output (Tan et al., 2021; Zhang et al., 2022; Ran et al., 2023a). However, the shallow coal resources are gradually exhausted, and the number of deep coal mines grows by years with the increase in the mining intensity (Zou et al., 2022b; Huang et al., 2023a; Zhao et al., 2023a; Sun X. Y. et al., 2023). Some coal mines that are originally not prone to rockburst have turned into rockburst-prone mines. In such context, rockburst has become and will continue to be one of the main disasters that restrict safe and efficient mining in China (Pan et al., 2013; Jiang et al., 2018; Liang et al., 2023). According to statistics, damage caused by 87% of rockburst is found in roadways, and rockburst disasters in roadways have become increasingly severe and frequent. Hence, rockburst disasters in roadways have become one of the main challenges that hinder safe production of coal mines (Xu et al., 2021; Dai et al., 2022; He and Wang, 2023; Wang et al., 2023). Rockburst in roadways may cause not only serious economic loss and casualties but also extremely negative social impact (Gong et al., 2022; Wang et al., 2022; Liu et al., 2023). In addition, the frequent occurrence of rockburst disasters in roadways in the coal industry is incompatible with the theme for harmonious and stable development of the current society (Zou et al., 2022a; Huang et al., 2023b), which restricts the further development of the coal industry (Tan Y. L. et al., 2023; Zhao et al., 2023b; Zhang C. L. et al., 2023).

The mining disturbance is an important factor that induces rockburst in roadways (Li et al., 2020; Ye et al., 2022). Litwiniszyn (2009) regarded rockburst as a result of an impact wave released by gravity-induced fractures of strata overlying a chamber. Li et al. studied the mechanical properties of hard rocks under dynamic-static loading by carrying out laboratory dynamic-static loading tests and simulated the rockburst induction mechanism by dynamic disturbances under high stress (Lei et al., 2005; Li et al., 2013). Lu et al. (2008) explored the impact failure law of roadway surrounding rocks under stress waves through numerical simulation and described the sudden failure process of spalled thin layers during rockburst in roadways. Afterward, Lu et al. (2008) investigated the formation process of spalling structures in roadway surrounding rocks under influences of disturbing stress waves, spalling failure phenomena in roadways induced by stress waves, and energy criteria for impact failure of roadways. Zhang et al. (2017) divided the coal wall into shallow plastic coal and deep subelastic coal along the vertical direction. The shallow plastic coal confines the subelastic coal. If the coal–rock contact surface is smooth enough, it is favorable for reducing the rockburst risk; if the contact surface is rough, it increases the rockburst risk. Characteristics of two focuses (mining-induced roof fracture and fault slip) and their influences on roadway surrounding rocks were studied (Wei et al., 2010; Hu et al., 2013). Aiming at characteristics of rockburst near faults, Cai et al. (2014) put forward a fault-induced rockburst mechanism characterized by one mining disturbance, two loads, interaction of three objects, and four failure modes. By studying typical rockburst cases, Pan et al. (2012) analyzed the rockburst evolution process, revealed three evolution stages (rockburst start-up, energy transfer, and rockburst occurrence), and obtained the material–structure dynamic failure mechanism for rockburst start-up. Linkov (1996) considered rockburst as the failure caused by softening and flowing deformation of coal–rock mass, and mining causes the coal–coal boundary, spatial structures of coal–rock mass, stress state, and elastic energy distribution to all change with time (Ran et al., 2023b; Zhang et al., 2023b; Chen et al., 2023; Zou et al., 2023). Therefore, the occurrence of rockburst has close temporal and spatial relationships with mining and is a result of the joint action of multiple temporal and spatial parameters. By carrying out microseismic tests, Gao et al. (2007) studied the energy attenuation factor during propagation of shock waves in different media and explored the fracture and failure mechanism of composite roof based on fracture mechanics and elastic–plastic mechanics. On this basis, three conditions related to the bearing capacity, deformation, and energy for impact failure of roadways were deduced, and the evolution process of six cracks (one horizontal and five vertical ones) in the roadway roof during rockburst under dynamic impact loads was expounded (Gao et al., 2017). Zhao et al. (2003) considered that huge elastic energy is accumulated in coal under triaxial stresses. The energy consumed by the failure of coal–rock mass under triaxial stresses is far larger than the energy needed for failure under uniaxial stress (Li et al., 2023; Ye et al., 2023). Once damage initiates in the coal–rock mass under triaxial stresses, the stress state of coal–rock mass is rapidly adjusted from biaxial to uniaxial stress states (Ma et al., 2023). The energy consumed by failure in the uniaxial stress state is the minimum energy needed for the failure of coal–rock mass, and the residual energy is the main energy factor that induces rockburst.

In summary, scholars in China and abroad studied the occurrence mechanism of rockburst mainly based on coal–rock properties, force sources, and mining (Du et al., 2022; He et al., 2022; Huang et al., 2022; Lou et al., 2023). However, there is little research conducted on energy evolution during rockburst development in deep roadway surrounding rocks under high static elastic energy. There is a lack of critical energy criteria for structural instability of surrounding rocks of rockburst-prone roadways, and the existing mechanism for controlling rockburst in roadways is ambiguous. In

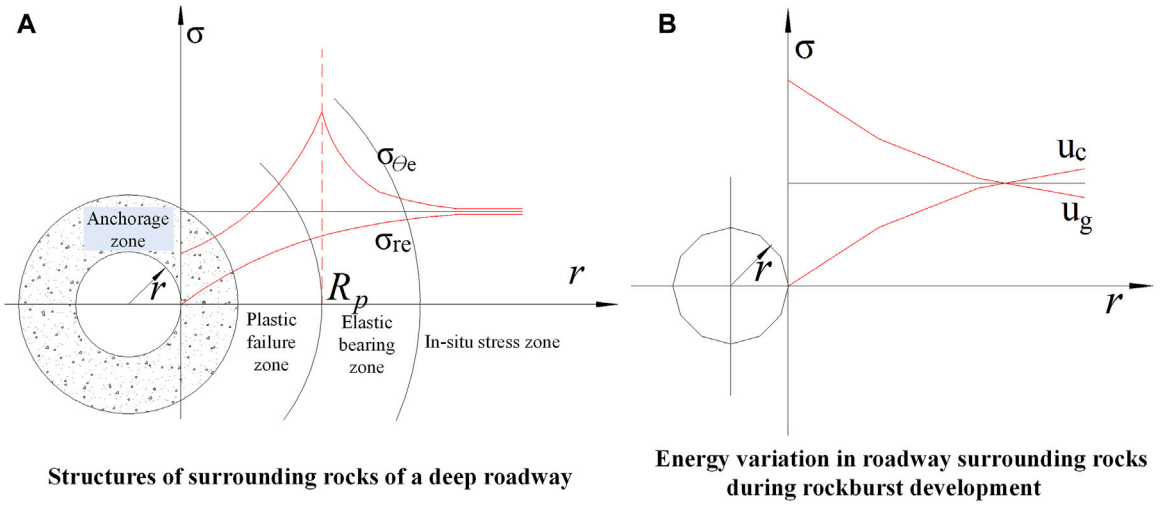

FIGURE 1
Structures and the energy evolution model of roadway surrounding rocks. **(A)** Structures of surrounding rocks of a deep roadway; **(B)** Energy variation in roadway surrounding rocks during rockburst development.

view of this, energy evolution during rockburst development in the elastic bearing zone and energy conversion characteristics in the plastic failure zone were studied based on the theory of elastic mechanics combining with structural characteristics of deep roadway surrounding rocks in coal mines. Influences of energy dissipation in coal–rock mass and support on the rockburst occurrence were analyzed combined with the state equation of rockburst. Based on the theory of rockburst start-up and the energy theory, critical energy criteria for structural instability of roadway surrounding rocks under static and dynamic loading were deduced. Using the FLAC^{3D} numerical simulation software, influences of the mining depth and coal pillar width on the elastic energy field in surrounding rocks of rockburst-prone roadways were revealed. Changes in the peak elastic energy density of roadway surrounding rocks and its peak point with the width of protective coal pillars in roadways and the asymmetric distribution of the elastic energy field in roadway surrounding rocks were analyzed. In this way, the occurrence mechanism of rockburst deep in coal mines was unveiled from the perspective of energy in structures of deep roadway surrounding rocks in coal mines.

2 Theoretical analysis of energy evolution in structures of deep roadway surrounding rocks during rockburst development

To analyze energy evolution in structures of deep roadway surrounding rocks during rockburst development, it is assumed that a roadway is located in a uniform stress field with the stress of σ0 before excavation; after excavation and support of the roadway, the surrounding rock structures are composed of four parts, namely, an anchorage zone, a plastic failure zone, an elastic bearing zone, and an *in situ* stress zone, as displayed in Figure 1.

2.1 Energy evolution during rockburst development in the elastic bearing zone

For the elastic bearing zone of the deep roadway, it is supposed that the minimum and maximum horizontal distances from the elastic bearing zone to the roadway boundary are separately R_p and l. The inner energy variation ΔU is solved directly using the elastic mechanics combined with the stress and displacement (Chen and Dou, 2008).

$$\Delta U = \frac{2\pi E}{1+\mu} R_p^2 u_{R_p} du_{R_p} \left(\frac{1}{R_p^2} - \frac{1}{l^2} \right), \tag{1}$$

where σ_{R0} and u_{Rp} represent the radial stress and displacement at the radius R_p of the plastic failure zone, respectively; μ and E denote the Poisson's ratio and elastic modulus of the roadway surrounding rocks, respectively.

According to Eq. 1, du_{Rp} is a linear function of dR_p. When dR_p = 0, the inner energy variation is 0 if the stress and support conditions of roadway surrounding rocks and the range of plastic failure zone remain unchanged; if $dRp > 0$, when changing the stress and support conditions of roadway surrounding rocks and enlarging the range of the plastic failure zone, the energy in the elastic bearing zone of roadway surrounding rocks begins to change. Therefore, energy is absorbed and accumulated in the elastic bearing zone when the coal–rock mass in the zone is affected by the mining disturbance.

Meanwhile, when not influenced by the mining disturbance, the roadway surrounding rocks in the elastic bearing zone are always stable and such state remains unchanged. That is, no energy is dissipated. Whereas, energy release from roadway surrounding rocks is a result of fracture propagation in the elastic bearing zone of surrounding rocks and accumulation of plastic deformation to a certain degree. Therefore, energy in the elastic bearing zone of roadway surrounding rocks can only change unidirectionally under external loads, that is, be absorbed. The following two energy-absorbing modes are mainly involved:

(1) When the roadway surrounding rocks are disturbed by mining, energy is absorbed and accumulated in the coal–rock mass in the elastic bearing zone, which serves as the propagation media of the external disturbance energy to transfer and release energy to shallow roadway sidewalls.
(2) With the enlarging radius of the plastic failure zone, the constraint changes for some coal–rock mass at the interface between the elastic bearing zone and plastic failure zone. The high tangential stress on the boundary is adjusted rapidly, and the energy accumulated in the elastic bearing zone is released instantaneously. This causes the energy released during roadway excavation to transfer to the deep space in the roadway and further induces energy accumulation in the coal–rock mass in the elastic bearing zone.

Similarly, when energy is released by the coal–rock mass in the *in situ* stress zone under the mining disturbance, coal–rock mass therein and in the elastic bearing zone both serve as the propagation media of external energy toward shallow roadway sidewalls and, thus, play a role in energy transfer.

2.2 Energy conversion characteristics in the plastic failure zone

Supposing that the roadway surrounding rocks are homogeneous, the elastic strain energy U_e accumulated in unit volume of coal–rock mass before excavation is calculated as follows:

$$U_e = \frac{3\sigma_0^2(1-2\mu)}{2E}. \tag{2}$$

After excavation, energy is accumulated in the shallow part of the roadway, where structures of the surrounding rocks are changed. Under the condition, the elastic strain energy U_P in unit volume of coal–rock mass in the plastic failure zone is calculated as follows:

$$U_P = \frac{\sigma_0^2\left[3(1-2\mu)+\frac{2(1+\mu)a^4}{r^4}\right]}{2E}, \tag{3}$$

where a is the roadway radius; r is the radius of the *in situ* stress zone of roadway surrounding rocks.

A comparison of Eqs. (2) and (3) shows that $U_P > U_e$. According to the triaxial compression tests, certain strain energy can be stored in coal–rock mass under the confining pressure (Liang et al., 2022). As the confining pressure increases, the ultimate strain energy U_P stored in the coal–rock mass ramps up; if the confining pressure is left unchanged, the harder or more intact the coal–rock mass is or the fewer the joints and fractures are in coal–rock mass, the higher the U_P. In the meantime, after excavating the roadway, the confining pressure is low in shallow surrounding rocks and is 0 around the roadway, and the ultimate strain energy stored in the fractured zone is low. As a result, the elastic strain energy that should be accumulated around the roadway is transferred to the deep coal–rock mass. With the growing distance from the roadway boundary, the elastic deformation energy stored in the deep coal–rock mass of the roadway gradually recovers to that before excavation again (elastic strain energy U_e). The energy release and transfer characteristics in roadway surrounding rocks during rockburst development are shown in Figure 1B.

In the near field of the roadway, mining induces redistribution of stress and energy in the rocks and causes energy transfer to the deep part, where coal–rock mass is plastically deformed. The stress state changes from triaxial to biaxial and even uniaxial one. According to the minimum energy principle, the energy needed for failure under uniaxial stress is far lower than that needed for failure under triaxial stresses. Therefore, the ultimate strain energy U_P declines abruptly. If the energy accumulated in the roadway surrounding rocks exceeds the energy dissipation U_k to overcome the failure, there is residual energy. Part of the residual energy is converted into kinetic energy for ejecting coal–rock mass, which can be further absorbed by the support or form kinetic energy; the other is converted into other dissipated energies such as acoustic energy and thermal energy. Assuming that the total energy input by the work done by external forces is U, its value is the deformation energy accumulated in all rock units in the rock system under triaxial stresses. Because other dissipated energies including acoustic energy are relatively low, if they are ignored, the state equation of rockburst of coal–rock mass is expressed as follows:

$$U = \frac{1}{2}mv^2 + U_k + U_c, \tag{4}$$

where m is the mass of the ejected coal–rock mass, v is the initial impact velocity of coal–rock mass, and U_c is the energy absorbed by the support.

According to Eqs. (3) and (4), the greater the energy accumulated in coal–rock mass after roadway excavation is, the higher the rockburst proneness will be. Enhancing the energy dissipation U_k of roadway surrounding rocks themselves and increasing the absorbed energy U_c of the support to some extent can limit the impact and ejection velocity of coal–rock mass, thus inhibiting the occurrence of rockburst.

Meanwhile, the energy in the elastic bearing zone and plastic failure zone of roadway surrounding rocks does not change in a certain time period after excavation, while it is affected by the disturbance of the external energy field. It is mainly shown as tremors induced by fracture of hard roofs and shear dislocation of faults, which disturb the near-field coal–rock mass in the roadway. The disturbances to structures of roadway surrounding rocks mainly include energy transfer, damage by stress waves, and weakening of support.

(1) Energy transfer: Energy is transferred outward from the focus to the surrounding area of the roadway. Under the effect of the transfer media, the energy is attenuated, and some energy is absorbed by the transfer media. Because the near-field structures of the roadway exert a small attenuation effect on the external disturbance energy, the energy is still high after attenuation. Rockburst may occur if Eq. 4 is satisfied.
(2) Damage by stress waves: Because external energy is applied to roadway surrounding rocks as compressed loading waves, which form reflected unloading waves in the pre-existing and secondary fractures in coal–rock mass and on the surface of roadway surrounding rocks, the reflected unloading waves are interacted with the compressed wave tail and reflected to form tensile stress waves. If the dynamic tensile–shear fracture criterion is met, fracture development is promoted so that the plastic zone of roadway surrounding rocks expands

abruptly, thus causing facture and ejection of coal–rock mass on the roadway surface to trigger rockburst.

(3) Weakening of support: Due to the interaction between support and surrounding rocks, disturbances of impact stress waves may result in fracture propagation in the structures of surrounding rocks. If the impact load is too large, the support fails when it absorbs energy that exceeds the allowable energy of deformation, thus failing to play its role in stably supporting the structures of roadway surrounding rocks. This triggers deep energy release and, therefore, rockburst disasters in the roadway.

2.3 Critical energy criteria for structural instability of roadway surrounding rocks

According to characteristics of energy sources that trigger rockburst in roadways, such rockburst can be divided into three types: the static load-type, dynamic load-type, and dynamic load-induced ones (Pan et al., 2012). Energy that causes static load-type rockburst in roadways sources from the static elastic energy stored in the elastic zone of roadway surrounding rocks during or after roadway excavation. For dynamic load-type rockburst in roadways, the elastic energy stored in the elastic zone of roadway surrounding rocks can be ignored, and the main energy source is the mining-induced external disturbance energy, which is non-steady and high. Part of energy causing dynamic load-induced rockburst in roadways sources from the elastic energy in the elastic zone of roadway surrounding rocks, and the other is the external disturbance energy. The two act together to induce rockburst in roadways. Under the condition, the dynamic energy is probably low and only functions as the starting condition for rockburst.

2.3.1 Critical energy characteristics in structures of roadway surrounding rocks under static loading

According to the theory of rockburst start-up, rockburst is composed of three stages, namely, rockburst start-up, energy transfer, and rockburst occurrence. The development of static elastic deformation energy is a necessary condition for the rockburst start-up stage. The energy density at any point in deep roadway surrounding rocks has a square relationship with the stress.

The occurrence of rockburst is a dynamic failure process, in which energy conversion follows the minimum energy principle for dynamic failure of rocks. That is to say, once damage initiates in rocks, the stress state of rocks changes rapidly from the triaxial to biaxial and finally uniaxial stress state. The failure criterion follows the uniaxial compression or shear failure criterion (Zou and Jiang, 2004):

(1) The failure criterion under uniaxial compression is $\sigma > \sigma_c$, and the energy consumption is $u_1 > \sigma_c^2/2E$, in which σ_c is the uniaxial compressive strength of rocks

(2) The failure criterion under uniaxial shear is $\tau > \tau_c$, and the energy consumption is $u_1 > \tau_c^2/2G$, in which τ_c and G are the shear strength and shear modulus of rocks, respectively

After rockburst start-up in the coal–rock mass, if energy release U_0 in the rockburst start-up zone is larger than energy consumption U' in the energy transfer and rockburst occurrence stages, then rockburst occurs, that is,

$$U_0\text{-}U' > 0. \tag{5}$$

The energy consumption in the energy transfer and rockburst occurrence stages mainly includes the energy for damaging coal–rock mass in the energy transfer process, refraction of stress waves, energy consumed by reflection, and energy absorbed by the support, that is,

$$U_0 = (u\text{-}u_1)V_0, U' = u_c V' + U'', V' = R_0 S, \tag{6}$$

where U_0 is the energy release in the rockburst start-up zone; U' is the energy consumption in the energy transfer process; u_1 is the energy density consumed in the rockburst start-up zone after start-up; V_0 is the volume of coal–rock mass that releases energy in the rockburst start-up zone; u_c is the average energy-dissipating capacity of coal–rock mass in the energy transfer process of rockburst; V' is the volume of coal–rock mass involved in energy dissipation in the energy transfer process of rockburst; U'' is the energy absorbed by the support system; R_0 is the distance from the rockburst start-up zone to the rockburst occurrence zone; and S is the average cross-sectional area of coal–rock mass involved in the energy transfer process of rockburst.

Therefore, under the joint action of the elastic strain energy stored in deep roadway surrounding rocks, energy release in the rockburst start-up zone, and energy in the energy transfer and consumption stages, the critical energy criterion for structural instability of structures of roadway surrounding rocks under static loading is given as follows:

$$\left\{\frac{k^2}{2E}\left[1 + {\lambda_x}^2 + {\lambda_y}^2 - 2\mu\left(\lambda_x + \lambda_y + \lambda_y\lambda_x\right)\right]\gamma^2 z^2 - \sigma_c^2\right\}V_0 - u_c R_0 S - U'' > 0. \tag{7}$$

If Eq. 7 is established, static load-type rockburst will occur in roadways.

The criterion was verified by an example. Rockburst occurred at 13 p.m. on 21 August 2008 when mining the lower roadway in the 21141 working face to 660 m in Qianqiu Coal Mine (Henan Province), and the damage range was 560–650 m to the opening of the roadway. The rockburst is a typical example of static load-type rockburst in roadways. When mining the lower roadway to 660 m, the stress concentration factor was large, and the static elastic energy was extremely high in the area due to tectonic influences. As the tunneling head advanced, the distance R0 from the mining space to the elastic zone with high static loads shortens, thus reaching the energy condition for occurrence of rockburst, which verifies the correctness of the criterion in Eq. 7.

According to Eqs. (3) and (7), rockburst in roadways can be prevented from three aspects when the burial depth of roadways and properties of coal–rock mass cannot be changed. The first is to reduce the stress concentration factor k. Because the impact energy is directly proportional to the square of the stress concentration factor k, reducing k can effectively decrease the impact energy. The second is to enlarge the distance from the rockburst start-up zone to the rockburst occurrence zone by taking artificial control measures. The third is to enhance the energy-absorbing capacity of the support, that is, improving U''.

2.3.2 Critical energy characteristics of structures of roadway surrounding rocks under dynamic loading

The energy sources for rockburst in roadways under dynamic loading include the elastic energy in the elastic zone of roadway surrounding rocks and the external disturbance energy. The two act together to trigger rockburst in roadways. After excavating a roadway, the stable static elastic deformation energy U_0 has been stored in the surrounding rocks, which, however, cannot meet the energy condition for rockburst start-up. With the advance of the working face, the disturbance energy $U_{\mathrm{d}}{}^0$ released at the moment of fracture of hard roof or fault slip and disturbance energy U_{d} transferred to the area with relatively stable and high elastic deformation energy density are superimposed with the relatively stable static elastic energy. As a result, the area becomes the rockburst start-up zone in the first stage of rockburst. The energy criterion for rockburst is expressed as follows:

$$U_0 + U_{\mathrm{d}}\text{-}U' > 0. \tag{8}$$

When the disturbance energy U_d^0 is transferred to the roadway surrounding rocks, the residual disturbance energy U_d is expressed as follows:

$$U_{\mathrm{d}} = \left(U_{\mathrm{d}}^0 \cdot d\right)^{-n}. \tag{9}$$

Combining with Eqs. (3) and (7), the critical energy criterion for structural instability of roadway surrounding rocks under dynamic loading is given as follows:

$$\left\{\frac{k^2}{2E}\left[1 + {\lambda_x}^2 + {\lambda_y}^2 - 2\mu\left(\lambda_x + \lambda_y + \lambda_y\lambda_x\right)\right]\gamma^2 z^2 - \sigma_{\mathrm{c}}^2\right\} V_0 + U_d^0 d^{-\eta} - u_c R_0 S - U'' > 0, \tag{10}$$

where d is the distance from the dynamic focus to the rockburst start-up zone and η is the disturbance energy attenuation factor.

If Eq. 10 is established, the dynamic load-type or dynamic load-induced rockburst will occur. The rockburst that occurred on 8 April 2018 in Menkeqing Coal Mine (the Inner Mongolia Autonomous Region) and on 9 June 2019 in Longjiabao Coal Mine (Jilin Province) both belong to dynamic load-induced rockburst.

3 Energy evolution in surrounding rocks of rockburst-prone roadways at different mining depths during rockburst development

In accordance with engineering and geological conditions of Menkeqing Coal Mine, FLAC^{3D} numerical simulation software was adopted to simulate energy evolution in surrounding rocks of rockburst-prone roadways at different mining depths during rockburst development. Considering the calculation accuracy and speed, the model with dimensions of 800 m × 800 m × 240 m (width × length × height) contained 1,394,200 grids and 1,522,018 nodes. The cross-sectional area of the driving roadway was 6.0 m × 5.0 m (width × height). The roadway was located in the center of the model. In static calculation, the displacements of left and right boundaries were fixed; the bottom was a boundary with fixed displacement, while uniform stress was applied onto the upper free boundary, on which loads of overlying strata were applied to simulate the elastic energy evolution at five mining depths, namely, 400, 600, 800, 1,000, and 1,200 m.

The Mohr–Coulomb model was used as the constitutive model. The mechanical parameters of coal–rock mass were converted from laboratory mechanical parameters of rocks. The elastic modulus, cohesion, and tensile strength were one-fifth to one-third of the laboratory test values, while Poisson's ratio is 1.2–1.4 times of the blocks. The physical and mechanical parameters used in the numerical simulation are listed in Table 1.

According to the aforementioned theoretical analysis and Eq. 12, the built-in FISH language of FLAC^{3D} was adopted to calculate the elastic deformation energy of elements.

If the principal stress is used to represent the principal strain and supposing that the coal–rock mass follows the generalized Hooke law, each principal stress in any element of coal–rock mass has the following relationship with the principal strain:

$$\begin{aligned}\varepsilon_1 &= \frac{1}{E}\left[\sigma_1 - \mu\left(\sigma_2 + \sigma_3\right)\right], \varepsilon_2 = \frac{1}{E}\left[\sigma_2 - \mu\left(\sigma_1 + \sigma_3\right)\right],\\ \varepsilon_3 &= \frac{1}{E}\left[\sigma_3 - \mu\left(\sigma_2 + \sigma_1\right)\right],\end{aligned} \tag{11}$$

where σ_1, σ_2, and σ_3 represent three principal stresses in the x-, y-, and z-direction, respectively; ε_1, ε_1, and ε_3 are strains corresponding to the three principal stresses, respectively; then,

$$u = \frac{\left[\sigma_1^2 + \sigma_2^2 + \sigma_3^2 - 2\mu\left(\sigma_1\sigma_2 + \sigma_1\sigma_3 + \sigma_3\sigma_2\right)\right]}{2E}. \tag{12}$$

To unveil influences of the mining depth on energy evolution in surrounding rocks of rockburst-prone roadways during rockburst development, the 3102 working face in Menkeqing Coal Mine was simulated. One side of the roadway in the working face was gob, and the width of the protective coal pillar was 30 m. The mining layout is displayed in Figure 2.

The post-processing software Tecplot was utilized to extract the strain energy density in roadway surrounding rocks. Combining with surfer software, cloud pictures for energy distribution and 3D cloud pictures for energy were drawn, as shown in Figure 3 and Figure 4, respectively.

Analysis of Figure 3 shows that as the mining depth increases, the energy density grows in the same zone of surrounding rocks. When the protective coal pillar is 30 m wide, the zone with large energy density is located in the roadway, and energy density is high in the retained coal pillar in the gob within a region 100 m behind the working face. The maximum energy density in entity coal in the working face is found at the end of the gob side near the 3101 working face. When the burial depth is 400 m, the maximum energy density is 280 kJ/m^3 in retained coal pillar in the gob within the region 100 m behind the gob, while it increases to 700, 1,500, 2,600, and 4,200 kJ/m^3 when the mining depths are 600, 800, 1,000, and 1,200 m, respectively. This indicates that as the burial depth of the roadway increases, the maximum energy density increases significantly and shows larger difference. Meanwhile, the energy density is only 190 kJ/m^3 in the region with the maximum energy density in surrounding rocks in the entity coal side of the working face at the burial depth of 400 m, while it grows to 500, 1,050, 1,900, and 2,800 kJ/m^3 when the mining depths are 600, 800, 1,000, and 1,200 m, respectively. Likewise, the deeper the

TABLE 1 Physical and mechanical properties used in numerical simulation.

Strata	Thickness/m	Density/kg.m^{-3}	Bulk modulus/GPa	Shear modulus/GPa	Poisson's ratio	Internal friction angle/°	Cohesion/MPa	Tensile strength/MPa
Silty mudstone	8	2,495	1.84	0.95	0.28	36	3.4	1.0
Sandy mudstone	8	2,430	1.15	0.47	0.32	36	3.0	0.8
Siltstone	7	2,495	1.84	0.95	0.28	36	3.4	1.0
Sandy mudstone	5	2,430	1.15	0.47	0.32	36	3.0	0.8
Siltstone	4	2,495	1.84	0.95	0.28	36	3.4	1.0
Sandy mudstone	5	2,430	1.15	0.47	0.32	36	3.0	0.8
Medium-grained sandstone	3	2,333	3.30	1.88	0.26	38	4.8	1.5
Siltstone	6	2,495	1.84	0.95	0.28	36	3.4	1.0
Sandy mudstone	5	2,430	1.15	0.47	0.32	36	3.0	0.8
Medium-grained sandstone	62.5	2,333	3.30	1.88	0.26	38	4.8	1.5
Siltstone	2	2,495	1.84	0.95	0.28	36	3.4	1.0
Sandy mudstone	5	2,430	1.15	0.47	0.32	36	3.0	0.8
Fine-grained sandstone	2	2,419	3.02	1.23	0.32	37	4.2	1.1
Siltstone	3	2,495	1.84	0.95	0.28	36	3.4	1.0
Fine-grained sandstone	18.5	2,419	3.02	1.23	0.32	37	4.2	1.1
Siltstone	4	2,495	1.84	0.95	0.28	36	3.4	1.0
3-1 coal	5	1,325	1.00	0.3	0.32	32	2.6	0.6
Sandy mudstone	10	2,430	1.84	0.95	0.28	36	3.4	1.0
Fine-grained sandstone	10	2,419	3.02	1.23	0.32	37	4.2	1.1

burial depth of the roadway is, the greater the difference in the maximum energy density will be. However, compared with energy density in the coal pillar, that in roadway surrounding rocks in the entity coal side of the working face is relatively small. Therefore, rockburst is likely to be triggered in the coal pillar in the deep gob-side roadway behind the stope, so retaining of coal pillars should be avoided during mining of the working face or pressure-relief measures should be taken to control energy accumulation in the coal pillar.

According to Figure 4, when retaining a protective coal pillar with the width of 30 m, the energy density is maximum in the coal pillar, and the larger the burial depth is, the more concentrated the energy accumulation will be. Figure 3 shows that the elastic energy density in the coal pillar is larger than that in the entity coal side of working face, and the elastic energy density in the coal pillar behind the working face is greater than that in the coal pillar ahead of the working face. The energy density is high in the retained coal pillar in the gob in the region 100 m behind the working face. The maximum elastic energy density in entity coal in the working face is found at the lower end of the working face, while it is lower than that in the coal pillar in the same region. Ahead of the working face, the elastic energy density gradually recovers to that in the *in situ* state beyond the range of advanced abutment pressure.

The energy density is high in the retained coal pillar in the region 100 m behind the stope, so rockburst is likely to occur in the region. However, even if rockburst occurs, it only slightly influences the safe production, so rockburst in the region is not discussed. When retaining a coal pillar of 30 m width, the energy density is high in the protective coal pillar in the range 50 m behind and 50 m ahead

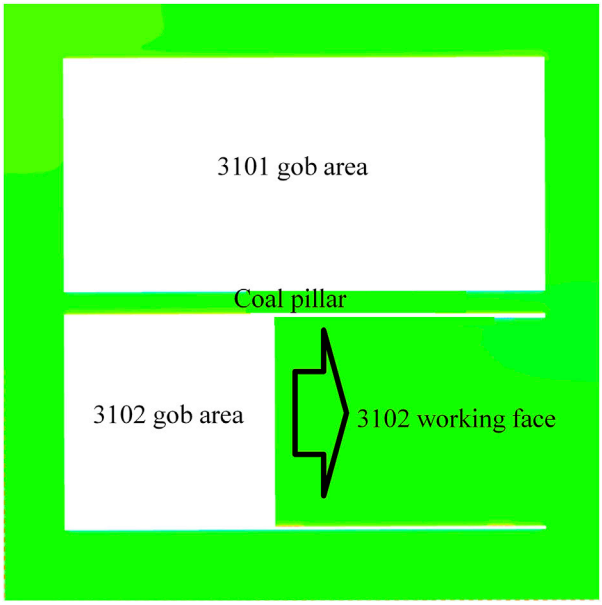

FIGURE 2
Schematic diagram of the simulated mining layout.

of the working face, so the region is most likely to experience rockburst according to the aforementioned analysis. For the protective coal pillar behind the working face, it can be damaged artificially to lose its bearing capacity so that elastic deformation energy cannot be stored therein. As a result, the energy cannot reach the condition for the occurrence of rockburst, which prevents the occurrence of rockburst. For the protective coal pillar ahead of the working face, its energy density is higher than that in the entity coal. The energy is distributed asymmetrically in roadway surrounding rocks, and the energy density is high in roadway surrounding rocks within the affected area of advanced abutment pressure, which gradually reduces to the value under conditions not being affected by the advanced abutment pressure. Therefore, the support technologies controlling structural stability of roadway surrounding rocks can be adopted according to energy characteristics in structures of surrounding rocks.

Additionally, the energy density in coal–rock mass ahead of the working face at different burial depths was extracted, and the changes are shown in Figure 5.

Analysis of Figure 5 shows that as the mining depth grows, the peak point of maximum energy density tends to shift to the coal ahead of the working face. As the mining depth varies from 400 m to 1,200 m, the peak point of maximum energy density gradually shifts inward from a position 5 m from the edge of the working face to a position 14 m from the working face. With the increase in burial depth, the energy density is more greatly influenced by the advanced abutment pressure of the working face, and the affected area is wider. With the increment in the mining depth, the maximum energy density in the affected area of advanced abutment pressure of the working face grows significantly. According to the critical energy criteria for structural instability of roadway surrounding rocks, the larger the mining depth is, the higher the proneness of coal–rock mass ahead of the working face to rockburst will be. This explains why the rockburst occurs more frequently with the increase in mining depth from the perspective of energy.

4 Energy evolution in surrounding rocks of rockburst-prone roadways during rockburst development under different coal pillar widths

To further study influences of the coal pillar width on energy evolution in surrounding rocks of rockburst-prone roadways during rockburst development, a roadway prototype with the gob in one side and the burial depth of 600 m in Menkeqing Coal Mine was taken as the background. Eight conditions with different widths of the protective coal pillar (4, 6, 8, 10, 15, 20, 30, and 60 m) were simulated, and the elastic energy density in roadway surrounding rocks was extracted and analyzed. According to Section 3, the rockburst is most likely to occur within and behind the affected area of advanced abutment pressure of the working face in the gob side. At the burial depth of 600 m, the peak point of elastic energy density in the entity coal in the working face is found at the position 10 m ahead of the working face. Therefore, the section mainly explores the distribution of elastic energy density in roadway surrounding rocks in the region 10 m ahead of the working face near the coal pillar side under different coal pillar widths.

The elastic energy density fields in roadway surrounding rocks under conditions of different widths of the protective coal pillar were extracted, as displayed in Figure 6. In the figure, positive values on the abscissa indicate the distance from the mining side of the roadway to a point inside entity coal in the working face, and the absolute values of negative values represent the distance from the coal pillar side to a point inside the coal pillar. This description is applied to similar cases below and not repeated.

Analysis of Figure 6 unveils that at the burial depth of 600 m, the peak elastic deformation energy density increases at first and then decreases with the increase in the width of the protective coal pillar. The energy density in the coal pillar gradually changes from one peak point to two, and the peak elastic energy density in the entity coal declines with the increase in coal pillar width.

To further clearly show changes in the elastic energy density field in roadway surrounding rocks under different widths of the protective coal pillar, change curves of energy under various coal pillar widths were obtained through pairwise comparison, as illustrated in Figure 7.

It is clearly seen from Figure 7A that when the protective coal pillar is 4 m wide, the peak elastic energy density in the coal pillar is very small (0.15×10^5 J/m^3), while that in the entity coal is 6.7×10^5 J/m^3. The peak point of elastic energy density in the entity coal is 9.5 m from the mining side of the roadway. When the width of the protective coal pillar is 6 m, the peak elastic energy densities in the coal pillar and entity coal are 0.32×10^5 and 6.3×10^5 J/m^3, respectively. Additionally, the peak point of elastic energy density in the entity coal is 10 m from the mining side of the roadway.

As displayed in Figure 7B, when the protective coal pillar is 8 m wide, the peak elastic energy densities in the coal pillar and entity coal are, respectively, 1.8×10^5 and 5.9×10^5 J/m^3, and the peak point is 10.5 m from the mining side of the roadway. If the protective coal pillar is 10 m wide, the peak elastic energy densities in the coal pillar

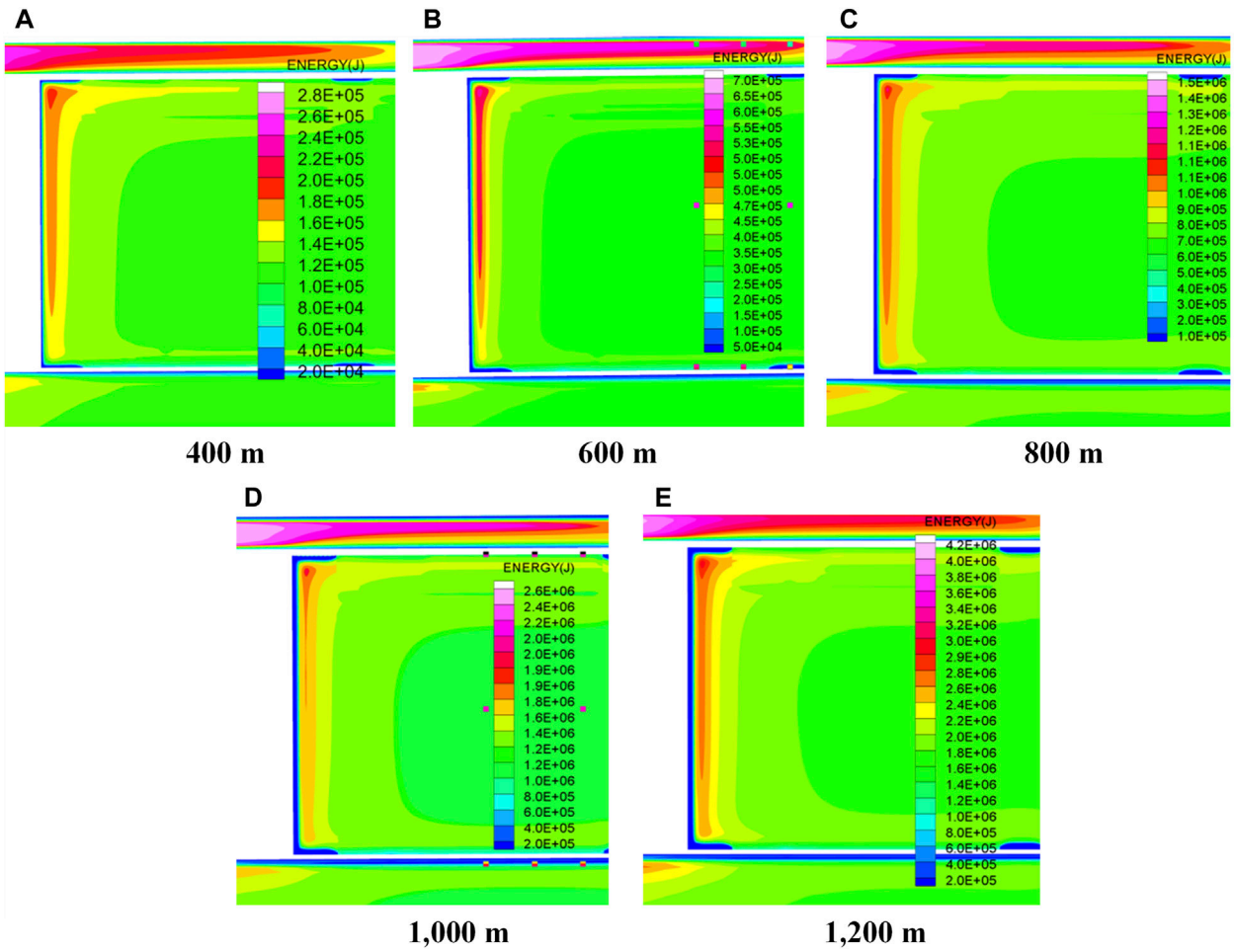

FIGURE 3
Cloud pictures for energy distribution in roadway surrounding rocks at different mining depths. **(A)** 400 m; **(B)** 600 m; **(C)** 800 m; **(D)** 1,000 m; **(E)** 1,200 m.

and entity coal are, respectively, 5.76×10^5 and 5.3×10^5 J/m^3, and the peak point of elastic energy density in the entity coal is 11 m from the mining side of the roadway.

According to Figure 7C, the peak elastic energy densities in the coal pillar and entity coal are, respectively, 7.1×10^5 and 5.14×10^5 J/m^3, and the peak point of elastic energy density in the entity coal is 12 m from the mining side of the roadway, when the protective coal pillar is 15 m wide. If the protective coal pillar is 20 m wide, the peak elastic energy densities in the coal pillar and entity coal are 6.0×10^5 and 4.7×10^5 J/m^3, respectively, and the peak point of elastic energy density in the entity coal is 12.5 m from the mining side.

It can be seen from Figure 7D that when the width of the protective coal pillar is 30 m, the peak elastic energy densities in the coal pillar and entity coal are 5.1×10^5 and 4.3×10^5 J/m^3, respectively, with the peak point of elastic energy density in the entity coal found at a position 13.5 m from the mining side of the roadway. When the protective coal pillar is 60 m wide, the elastic energy density in the coal pillar has two peaks: the one near the roadway side is small (3.77×10^5 J/m^3), while that near the gob side is large (4.40×10^5 J/m^3). The peak elastic energy density in the entity coal is 3.9×10^5 J/m^3, and its peak point is 15.5 m from the mining side.

As shown in Figure 6 and Figure 7, the energy field is asymmetrically distributed in roadway surrounding rocks, and its value and location of peak point are strongly correlated with the coal pillar width. On the whole, the wider the protective coal pillar, the lower the peak energy in the entity coal and the deeper the peak point shifts to the coal, which is more conducive to preventing rockburst. However, retaining a wide coal pillar may waste coal resources; if retaining a protective coal pillar narrower than 8 m, the elastic energy density is low in the coal pillar, while that is high in the entity coal. The peak energy density in the entity coal side of the roadway can be reduced by taking artificial control measures including drilling large-diameter boreholes for pressure relief and softening coal by water injection.

The peak points of elastic energy density and peak energy characteristics in the entity coal under different coal pillar widths are summarized in Figure 8.

As shown in Figure 8A, as the width of the protective coal pillar enlarges, the distance from the peak point of energy density to the roadway boundary enlarges abruptly at first and then slowly, with the critical coal pillar width for gentle change in the distance being 30 m. When the coal pillar width is 4 m, the peak point of elastic

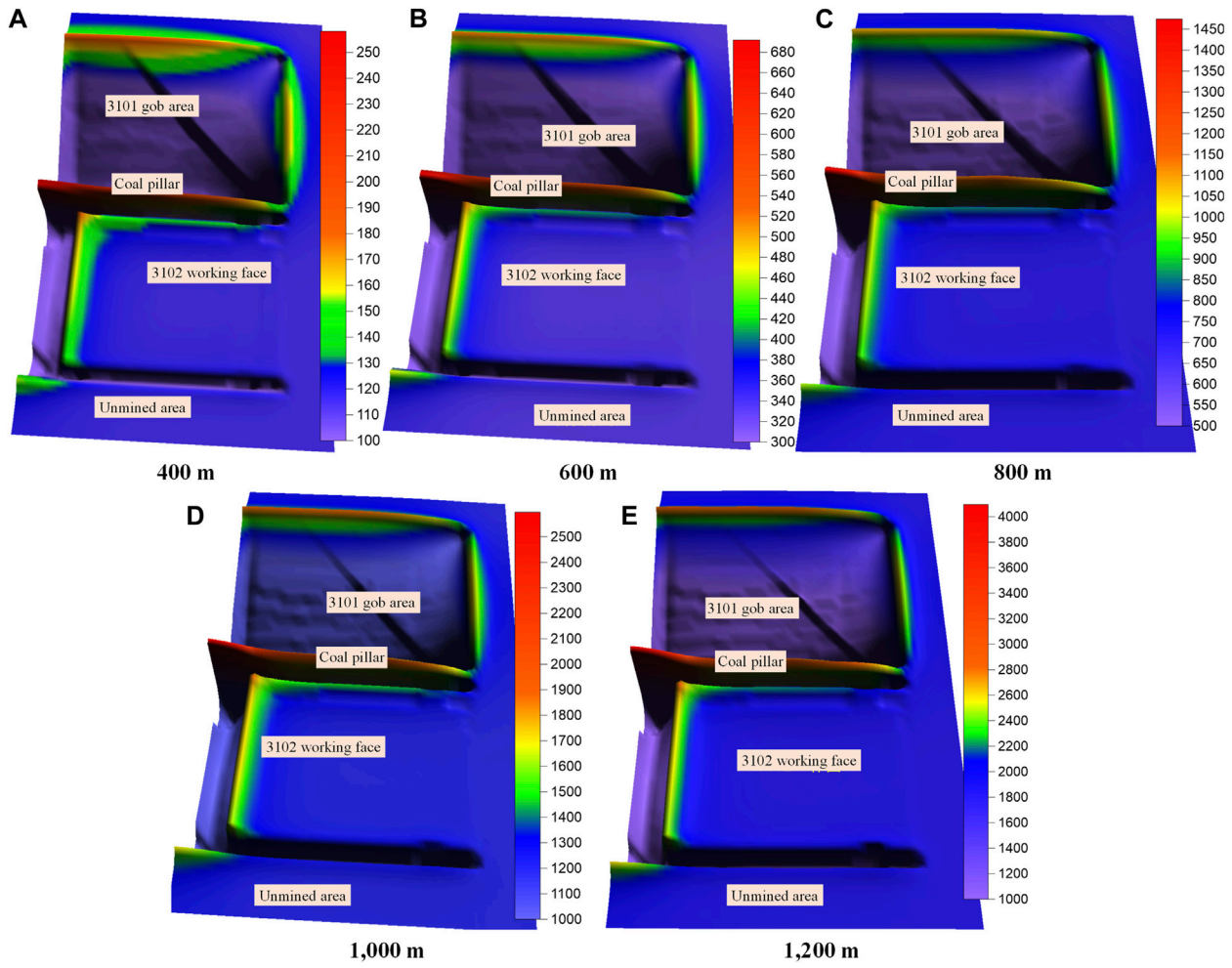

FIGURE 4
3D images for energy evolution in roadway surrounding rocks at different depths. **(A)** 400 m; **(B)** 600 m; **(C)** 800 m; **(D)** 1,000 m; **(E)** 1,200 m.

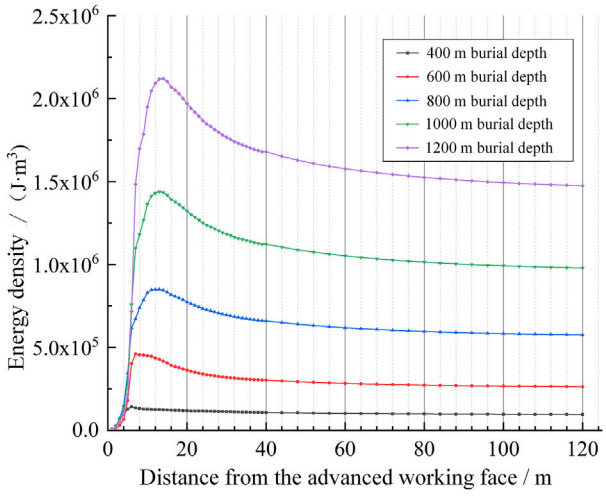

FIGURE 5
Inner elastic energy and density change curves of coal–rock mass ahead of the working face at different depths.

energy density in the entity coal is 9.5 m from the mining side of the roadway. As the width gradually enlarges to 60 m, the peak point gradually shifts to the position 15.5 m from the mining side. The change trend indicates that when the coal pillar width is smaller than 15 m, changes in the width significantly affect the location of peak point of elastic energy density in the entity coal, while the influence becomes gentle when the width is larger than 15 m.

Figure 8B depicts that when the width of the protective coal pillar is 4 m, the peak elastic energy density in the entity coal is 6.6×10^5 J/m^3, while it gradually declines to 3.90×10^5 J/m^3 when the width is 60 m. The change trend can be roughly divided into two stages: when the coal pillar width is smaller than 20 m, the peak energy density declines abruptly with the widening of the protective coal pillar; when the width is in the range of 20–60 m, reduction of the peak energy density flattens. It is predictable that the peak elastic energy density in the coal pillar will approximate to a value when the width of the protective coal pillar reaches a certain value.

In the meantime, changes in the elastic energy density in the coal pillar under conditions of different coal pillar widths were extracted, as displayed in Figure 9. It is evident that changes in the peak elastic energy density in the coal pillar with the coal pillar width can be roughly

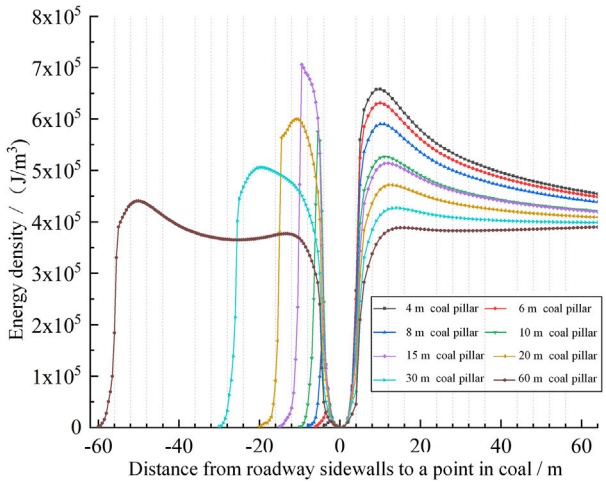

FIGURE 6
Variation law of elastic energy density fields in roadway surrounding rocks with different widths of protective coal pillar.

divided into four stages. The first is the slow increase stage of energy density: when the protective coal pillar is 4–6 m wide, the peak elastic energy density in the coal pillar increases slowly from the minimum (0.15×10^5 J/m^3) to 0.32×10^5 J/m^3. The second is the abrupt increase stage of energy density: when the width of the protective coal pillar is in the range of 6–13 m, the peak elastic energy density in the coal pillar grows abruptly from 0.32×10^5 to 7.70×10^5 J/m^3. The third is the abrupt decrease stage of energy density: when the coal pillar width is in the range of 13–20 m, the peak elastic energy density in the coal pillar reduces abruptly to 6.0×10^5 J/m^3. The fourth is the slow decrease stage of energy density: when the coal pillar width is larger than 20 m, the peak elastic energy density in the coal pillar declines slowly with the increase in width. It is predictable that the peak elastic energy density in the coal pillar may approximate to a value when the width of the protective coal pillar reaches a certain value.

Meanwhile, changes in the peak energy density in deep roadway surrounding rocks with the coal pillar width are summarized in Table 2.

As displayed in Table 2, the peak energy density in the entity coal gradually reduces from 6.6×10^5 to 3.9×10^5 J/m^3, and the distance from the peak point to the roadway boundary increases from 9.5 to

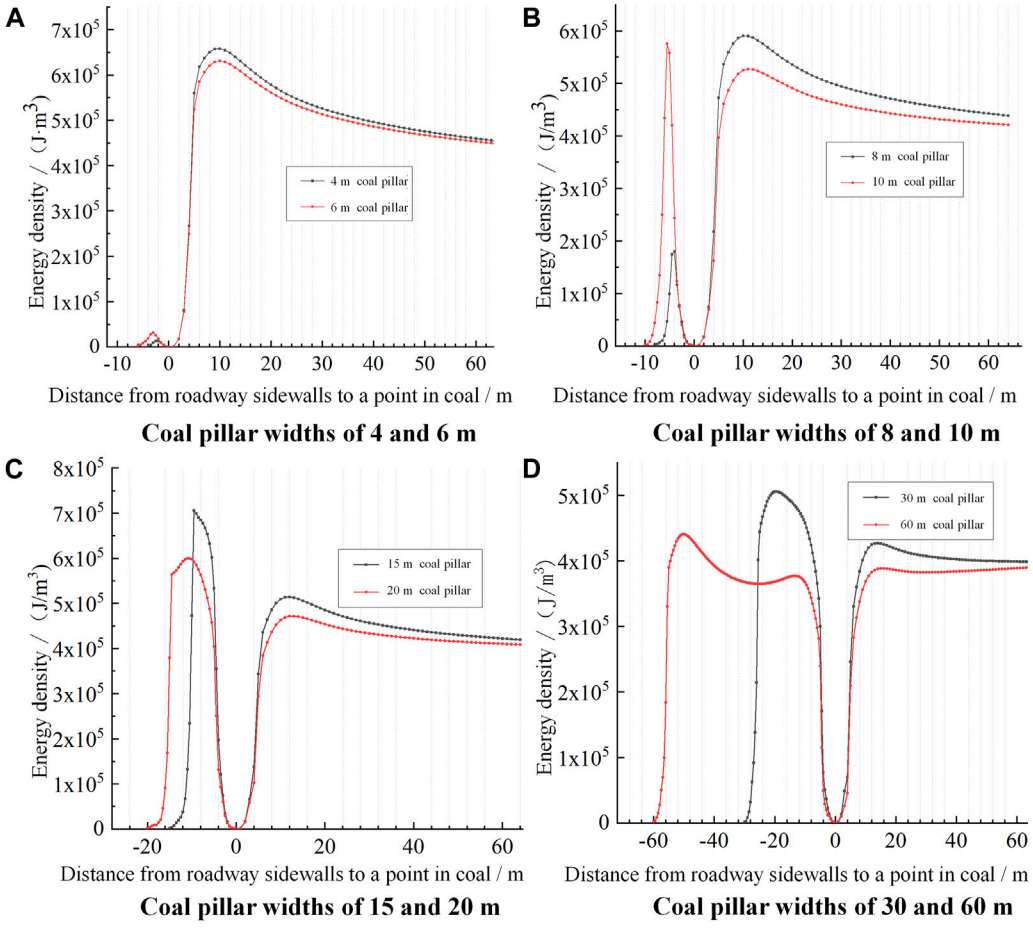

FIGURE 7
Variation law of elastic energy density fields in roadway surrounding rocks with different widths of protective coal pillar. **(A)** Coal pillar widths of 4 and 6 m; **(B)** Coal pillar widths of 8 and 10 m; **(C)** Coal pillar widths of 15 and 20 m; **(D)** Coal pillar widths of 30 and 60 m.

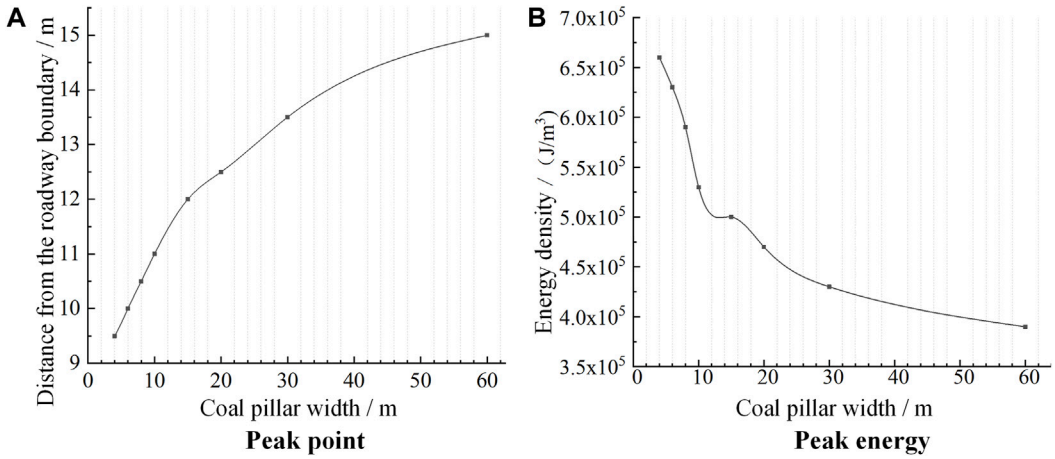

FIGURE 8
Peak point of inner elastic energy density in entity coal and the changes in peak energy.

TABLE 2 Peak energy density of deeply impacted roadway surrounding rocks with the coal pillar width.

Coal pillar width	4 m	6 m	8 m	10 m	15 m	20 m	30 m	60 m
Peak energy density in the entity coal/10^5J/m^3	6.6	6.3	5.9	5.3	5.14	4.70	4.30	3.90
Peak energy density in the coal pillar/10^5J/m^3	0.15	0.32	1.80	5.76	7.10	6.0	5.11	3.77
Distance from the peak energy density in entity coal to the coal wall/m	9.5	10.0	10.5	11.0	12.0	12.5	13.5	15.5

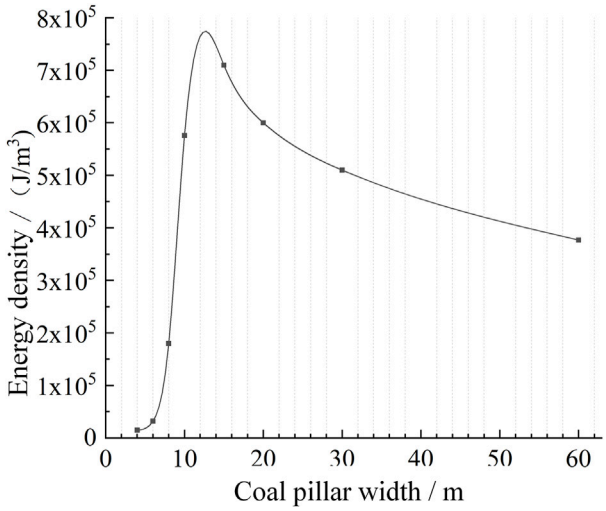

FIGURE 9
Variation law of the peak elastic energy density in coal pillars with the coal pillar width.

15.5 m with the increase in coal pillar width. On the contrary to changes in the peak energy density in the entity coal, the wider the coal pillar is, the higher the peak energy density in the coal pillar will be, which grows from 0.15 × 10^5 J/m^3 under the coal pillar width of 4 m to 3.77 × 10^5 J/m^3 when the width is 60 m.

Therefore, the elastic energy density is notably asymmetrically distributed in deep roadway surrounding rocks in the coal mine. Under action of structures of roadway surrounding rocks, the energy evolution during rockburst development in these structures differs remarkably under different coal pillar widths. To prevent rockburst in roadways, the support patterns suitable for deep rockburst-prone roadways should be proposed according to structural characteristics of deep roadway surrounding rocks and energy evolution characteristics during rockburst development in the coal mine.

5 Conclusion

The energy evolution characteristics during rockburst development in structures of deep roadway surrounding rocks were studied according to structural characteristics of deep roadway surrounding rocks in coal mines. FLAC3D numerical simulation software was utilized to analyze influences of the mining depth and coal pillar width on energy evolution in rockburst-prone roadways during rockburst development. The main conclusions include the following:

(1) Based on the theory of elastic mechanics, energy evolution during rockburst development in the elastic bearing zone and energy conversion characteristics in the plastic failure zone of roadway surrounding rocks were analyzed. According to the state equation of rockburst, influences of energy dissipation in coal–rock mass and support on rockburst were analyzed, and

disturbance characteristics of external energy on structures of roadway surrounding rocks were discussed. The research pointed out that with the enlargement of the affected area of the plastic failure zone, coal–rock mass in the elastic bearing zone only changes unidirectionally into energy absorption. Two energy-absorbing modes are involved, namely, energy absorption of propagation media of disturbance energy toward the roadway and energy transfer and accumulation for rockburst development. The coal–rock mass and stress state in the plastic failure zone change from the triaxial to biaxial and even uniaxial state, and the elastic strain energy reduces abruptly.

(2) Based on the theory of rockburst start-up and the energy theory, critical energy criteria for structural instability of roadway surrounding rocks under static and dynamic loading were deduced, taking energy release in the rockburst start-up zone larger than energy consumption during energy transfer and rockburst occurrence as the criterion. They are closely related to the elastic strain energy stored in deep roadway surrounding rocks and the energy absorbed by support systems. The impact energy in roadways is found to be directly proportional to the square of the stress concentration factor k. The occurrence of rockburst can be prevented by reducing the stress concentration factor, enlarging the distance from the rockburst start-up zone to the rockburst occurrence zone using artificial control measures, and enhancing the energy-absorbing capacity of the support.

(3) As the mining depth increases, the energy density in surrounding rocks grows in the same region. When the protective coal pillar is 30 m wide, the region with high energy density in the coal–rock mass is found in the roadway, and the energy density is high in the retained coal pillar in the gob in the region 100 m behind the working face. The maximum energy density in the entity coal in the working face is found at the end in the gob side near the previous working face. As the mining depth increases, the peak point of maximum energy density gradually shifts to the coal ahead of the working face. With increase in burial depth, the energy density is more remarkably affected by the advanced abutment pressure of the working face, and the larger the burial depth is, the wider the affected area will be. The maximum energy density in the coal–rock mass ahead of the working face exhibits an obvious increment with the increase in mining depth.

(4) At the same burial depth, the peak elastic energy density in the coal pillar increases at first and then decreases with the increase in coal pillar width. The energy density in the coal pillar changes from one peak point to two as the coal pillar width enlarges, and the peak elastic energy density in the entity coal decreases with the increase in width. As the coal pillar width enlarges, the distance from the peak point of energy density to the roadway boundary increases abruptly at first and then slowly, and the critical coal pillar width for the gentle change is 30 m. Changes in the peak elastic energy density in the coal pillar with the coal pillar width can be roughly divided into four stages: the slow increase stage, abrupt increase stage, abrupt decrease stage, and slow decrease stage of energy density. The elastic energy density in deep roadway surrounding rocks in the coal mine is obviously asymmetrically distributed. Under the action of structures of roadway surrounding rocks, the energy evolution during rockburst development differs greatly in these structures under different coal pillar widths.

Data availability statement

The original contributions presented in the study are included in the article/Supplementary Material; further inquiries can be directed to the corresponding authors.

Author contributions

ZX, ZC, and CL: writing–original draft and writing–review and editing. CF, HQ, WL, KG, HC, YX, and LY: data curation and writing–original draft.

Funding

The authors acknowledge financial support provided by the Science and Technology Development Fund Project of Coal Research Institute (Basic Fund), the National Natural Science Foundation of China (52074120, 52104131), and the Fundamental Research Funds for the Central Universities (3142019005, 3142017107).

Conflict of interest

The authors declare that the research was conducted in the absence of any commercial or financial relationships that could be construed as a potential conflict of interest.

Publisher's note

References

Cai, W., Dou, L. M., He, J., Liu, H. S., Li, Z. L., and Ding, Y. L. (2014). Mechanical genesis of Henan (China) Yima thrust nappe structure. *J. Central South Univ.* 21 (7), 2857–2865. doi:10.1007/s11771-014-2251-6

Chen, G. X., and Dou, L. M. (2008). Energy analysis of rock burst on excavated circular roadway under uniform pressure. *J. Min. Saf. Eng.* 25 (1), 27–31.

Chen, Z. H., Zou, Q. L., Gao, S. K., Zhan, J. F., Chen, C. M., Ran, Q. C., et al. (2023). Long-term evolution of overlying rock fractures in mined-out areas and its effect on gas flow conductivity. *Fuel* 353, 129213. doi:10.1016/j.fuel.2023.129213

Dai, J. H., Yang, J. H., Yao, C., Hu, Y. G., Zhang, X. B., Jiang, Q. H., et al. (2022). Study on the mechanism of displacement mutation for jointed rock slopes during blasting excavation. *Int. J. Rock Mech. Min. Sci.* 150, 105032. doi:10.1016/j.ijrmms.2021.105032

Du, F., Ma, J., Guo, X. F., Wang, T. F., Dong, X. H., Li, J. S., et al. (2022). Rockburst mechanism and the law of energy accumulation and release in mining roadway: a case study. *Int. J. Coal Sci. Technol.* 9 (1), 67. doi:10.1007/s40789-022-00521-0

Gao, M. S., Dou, L. M., Zhang, N., Mu, Z. L., Wang, K., and Yang, B. S. (2007). Experimental study on earthquake tremor for transmitting law of rockburst in geomaterials. *Chin. J. Rock Mech. Eng.* 26 (7), 1365–1371.

Gao, M. S., Liu, Y. M., Zhao, Y. C., Gao, X. J., and Wen, Y. Y. (2017). Failure mechanism of impact fracture of deep coal roadway roof and its dynamic manifestations. *J. China Coal Soc.* 42 (7), 1650–1655. doi:10.13225/j.cnki.jccs.2016.1464

Gong, F. Q., He, Z. C., and Jiang, Q. (2022). Internal mechanism of reducing rockburst proneness of rock under high stress by real-time drilling pressure relief. *Rock Mech. Rock Eng.* 55 (8), 5063–5081. doi:10.1007/s00603-022-02904-w

He, M. C., and Wang, Q. (2023). Rock dynamics in deep mining. *Int. J. Min. Sci. Technol.* 33 (9), 1065–1082. doi:10.1016/j.ijmst.2023.07.006

He, M. M., Zhao, J. R., Deng, B. Y., and Zhang, Z. Q. (2022). Effect of layered joints on rockburst in deep tunnels. *Int. J. Coal Sci. Technol.* 9 (1), 21. doi:10.1007/s40789-022-00489-x

Hu, S. B., Wang, E. Y., and Shen, R. X. (2013). Characteristics of dynamic disturbance response in deep coal and rock and its numerical analysis. *J. China Univ. Min. Technol.* 42 (4), 540–546.

Huang, L. K., He, R., Yang, Z. Z., Tan, P., Chen, W. H., Li, X. G., et al. (2023a). Exploring hydraulic fracture behavior in glutenite formation with strong heterogeneity and variable lithology based on DEM simulation. *Eng. Fract. Mech.* 278, 109020. doi:10.1016/j.engfracmech.2022.109020

Huang, L. K., Tan, J., Fu, H. F., Liu, J. J., Chen, X. Y., Liao, X. C., et al. (2023b). The non-plane initiation and propagation mechanism of multiple hydraulic fractures in tight reservoirs considering stress shadow effects. *Eng. Fract. Mech.* 292, 109570. doi:10.1016/j.engfracmech.2023.109570

Huang, L. Q., Si, X. F., Li, X. B., Gong, F. Q., and Luo, Y. (2022). Influence of maximum principal stress direction on the failure process and characteristics of D-shaped tunnels. *Int. J. Min. Sci. Technol.* 32 (5), 1125–1143. doi:10.1016/j.ijmst.2022.07.004

Jiang, F. X., Yang, G. Y., Wei, Q. D., Wang, C. W., Qu, X. C., and Zhu, S. T. (2018). Study and prospect on coal mine composite dynamic disaster real-time prewarning platform. *J. China Coal Soc.* 43 (2), 333–339. doi:10.13225/j.cnki.jccs.2017.4152

Lei, G. Y., Lu, A. H., and Mao, X. B. (2005). Numerical simulation on layered crack and failure of roadway under stress wave. *Rock Soil Mech.* 26 (09), 1477–1480.

Li, B., Yang, X., Yuan, Y., Liang, Y. P., Li, S. Q., Zhu, C. Q., et al. (2023). Experimental research on the influence of different factors on the behaviour of broken coal and rock particles during compaction. *Constr. Build. Mater.* 367, 130127. doi:10.1016/j.conbuildmat.2022.130127

Li, Q. M., Liang, Y. P., Zou, Q. L., and Li, Q. G. (2020). Acoustic emission and energy dissipation characteristics of gas-bearing coal samples under different cyclic loading paths. *Nat. Resour. Res.* 29 (2), 1397–1412. doi:10.1007/s11053-019-09508-2

Li, X. B., Yao, J. R., and Du, K. (2013). Preliminary study for induced fracture and non-explosive continuous mining in high-geostress hard rock mine-a case study of Kaiyang phosphate mine. *Chin. J. Rock Mech. Eng.* 32 (6), 1101–1111.

Liang, Y. P., Kong, F. J., Zou, Q. L., and Zhang, B. C. (2023). Effect of strain rate on mechanical response and failure characteristics of horizontal bedded coal under quasi-static loading. *Geomechanics Geophys. Geo-Energy Geo-Resources* 9 (1), 52. doi:10.1007/s40948-023-00587-3

Liang, Y. P., Ran, Q. C., Zou, Q. L., Zhang, B. C., and Hong, Y. (2022). Experimental study of mechanical behaviors and failure characteristics of coal under true triaxial cyclic loading and unloading and stress rotation. *Nat. Resour. Res.* 31 (2), 971–991. doi:10.1007/s11053-022-10022-1

Linkov, A. M. (1996). Rockbursts and the instability of rock masses. *Int. J. Rock Mech. Min. Sci. Geomechanics Abstr.* 33 (7), 727–732. doi:10.1016/0148-9062(96)00021-6

Litwiniszyn, J. (2009). Rarefaction shock waves, out bursts and consequential coal damage. *Int. J. Rock Mech. Min. Sci. Geomechanics Abstr.* 27 (6), 535–540. doi:10.1016/0148-9062(90)91004-Q

Liu, C. Y., Zhao, G. M., Xu, W. S., Meng, X. R., Liu, Z. X., Cheng, X., et al. (2023). Experimental study on failure characteristics of single-sided unloading rock under different intermediate principal stress conditions. *Int. J. Min. Sci. Technol.* 33 (3), 275–287. doi:10.1016/j.ijmst.2022.12.005

Lou, J. F., Gao, F. Q., Li, J. Z., Yuan, G. Y., and Sharifzadeh, M. (2023). Effect of dynamic loading conditions on the dynamic performance of MP1 energy-absorbing rockbolts: insight from laboratory drop test. *Int. J. Min. Sci. Technol.* 33 (2), 215–231. doi:10.1016/j.ijmst.2022.09.023

Lu, A. H., Yu, S. L., Qin, H., and Mao, X. B. (2008). Stability of layered crack structure in roadway surrounding rock under stress wave. *J. China Univ. Min. Technol.* 37 (6), 769–775.

Ma, T. F., Liu, H. H., Zou, Q. L., Kong, F. J., Ran, Q. C., and Wang, P. T. (2023). Damage evolution characteristics and deterioration mechanism of mechanical properties of sandstone subjected to drying-wetting cycles. *J. Mater. Res. Technol.* 23, 4591–4605. doi:10.1016/j.jmrt.2023.02.068

Pan, J. F., Mao, D. B., Lan, H., Wang, S. W., and Qi, Q. X. (2013). Study status and prospects of mine pessure bumping control Technology in China. *Coal Sci. Technol.* 41 (06), 21–25+41. doi:10.13199/j.cst.2013.06.27.panjf.012

Pan, J. F., Ning, Y., Mao, D. B., Lan, H., Du, T. T., and Peng, Y. W. (2012). Theory of rockburst start-up during coal mining. *Chin. J. Rock Mech. Eng.* 31 (3), 586–596.

Ran, Q. C., Liang, Y. P., Zou, Q. L., Hong, Y., Zhang, B. C., Liu, H., et al. (2023a). Experimental investigation on mechanical characteristics of red sandstone under graded cyclic loading and its inspirations for stability of overlying strata. *Geomechanics Geophys. Geo-Energy Geo-Resources* 9 (1), 11. doi:10.1007/s40948-023-00555-x

Ran, Q. C., Liang, Y. P., Zou, Q. L., Zhang, B. C., Li, R. F., Chen, Z. H., et al. (2023b). Characteristics of mining-induced fractures under inclined coal seam group multiple mining and implications for gas migration. *Nat. Resour. Res.* 32 (3), 1481–1501. doi:10.1007/s11053-023-10199-z

Su, E. L., Liang, Y. P., Chen, X. J., Wang, Z. F., Ni, X. M., Zou, Q. L., et al. (2023). Relationship between pore structure and mechanical properties of bituminous coal under sub-critical and super-critical CO2 treatment. *Energy* 280, 128155. doi:10.1016/j.energy.2023.128155

Sun, D. L., Liang, Y. P., Huang, X. C., and Ran, Q. C. (2023a). Progress and prospects of coalbed methane development and utilization in coal mining areas with large dip angle and multiple coal groups in Xinjiang. *Coal Sci. Technol.* 51 (S1), 161–171. doi:10.13199/j.cnki.cst.mcq2022-1325

Sun, X. Y., Ran, Q. C., Liu, H., Ning, Y. H., and Ma, T. F. (2023b). Characteristics of stress-displacement-fracture multi-field evolution around gas extraction borehole. *Energies* 16 (6), 2896. doi:10.3390/en16062896

Tan, P., Fu, S. H., Chen, Z. W., and Zhao, Q. (2023a). Experimental investigation on fracture growth for integrated hydraulic fracturing in multiple gas bearing formations. *Geoenergy Sci. Eng.* 231 (1), 212316. doi:10.1016/j.geoen.2023.212316

Tan, P., Jin, Y., and Pang, H. W. (2021). Hydraulic fracture vertical propagation behavior in transversely isotropic layered shale formation with transition zone using XFEM-based CZM method. *Eng. Fract. Mech.* 248, 107707. doi:10.1016/j.engfracmech.2021.107707

Tan, Y. L., Ma, Q., Liu, X. L., Liu, X. S., Elsworth, D., Qian, R. P., et al. (2023b). Study on the disaster caused by the linkage failure of the residual coal pillar and rock stratum during multiple coal seam mining: mechanism of progressive and dynamic failure. *Int. J. Coal Sci. Technol.* 10 (1), 45. doi:10.1007/s40789-023-00603-7

Wang, T. A., Zhai, Y., Gao, H., Li, Y. B., and Zhao, R. F. (2023). A novel binary effective medium model to describe the prepeak stress-strain relationship of combined bodies of rock-like material and rock. *Int. J. Min. Sci. Technol.* 33 (5), 601–616. doi:10.1016/j.ijmst.2022.11.007

Wang, X., Li, J. C., Zhao, X. B., and Liang, Y. (2022). Propagation characteristics and prediction of blast-induced vibration on closely spaced rock tunnels. *Tunn. Undergr. Space Technol.* 123, 104416. doi:10.1016/j.tust.2022.104416

Wei, M. Y., Wang, E. Y., Liu, X. F., Song, D. Z., and Zhang, Y. (2010). Numerical simulation of roof fracture induced by dynamic disturbance. *J. Min. Saf. Eng.* 27 (04), 532–536.

Wu, Q. F., Han, S. X., Li, S. S., Yu, M. G., Zheng, K., Li, H. T., et al. (2023). Explosive characteristics of non-uniform methane-air mixtures in half-open vertical channels with ignition at the open end. *Energy* 284, 128687. doi:10.1016/j.energy.2023.128687

Wu, Q. F., Yu, M. G., and Zheng, K. (2022). Experimental investigation on the effect of obstacle position on the explosion behaviors of the non-uniform methane/air mixture. *Fuel* 320, 123989. doi:10.1016/j.fuel.2022.123989

Xu, L., Gong, F. Q., and Luo, S. (2021). Effects of pre-existing single crack angle on mechanical behaviors and energy storage characteristics of red sandstone under uniaxial compression. *Theor. Appl. Fract. Mech.* 113, 102933. doi:10.1016/j.tafmec.2021.102933

Ye, C. F., Xie, H. P., Wu, F., and Li, C. B. (2022). Nonlinear creep properties and time-to-failure prediction of sandstone under saturated and dry conditions. *Environ. Earth Sci.* 81, 545. doi:10.1007/s12665-022-10666-5

Ye, C. F., Xie, H. P., Wu, F., and Li, C. B. (2023). Study on the nonlinear time-dependent deformation characteristics and viscoelastic-plastic model of shale under direct shear loading path. *Bull. Eng. Geol. Environ.* 82 (5), 189. doi:10.1007/s10064-023-03170-y

Zhang, B. C., Liang, Y. P., Zhao, Z. Y., Zou, Q. L., Zheng, H. L., Ning, Y. H., et al. (2023a). Effect of stress amplitude on mechanical and acoustic emission of sandstone under constant–cyclic loading. *Bull. Eng. Geol. Environ.* 82, 284. doi:10.1007/s10064-023-03307-z

Zhang, B. C., Liang, Y. P., Zou, Q. L., Ding, L. Q., and Ran, Q. C. (2023b). Experimental investigation into the damage evolution of sandstone under decreasing-amplitude stress rates and its implications for coalbed methane exploitation. *Environ. Earth Sci.* 82, 208. doi:10.1007/s12665-023-10825-2

Zhang, C. G., Ismet, C., Faham, T., and Bruce, H. (2017). Assessment of energy release mechanisms contributing to coal burst. *Int. J. Min. Sci. Technol.* 27 (1), 43–47. doi:10.1016/j.ijmst.2016.09.029

Zhang, C. L., Wang, P. Z., Wang, E. Y., Chen, D. P., and Li, C. (2023c). Characteristics of coal resources in China and statistical analysis and preventive measures for coal mine accidents. *Int. J. Coal Sci. Technol.* 10 (1), 22. doi:10.1007/s40789-023-00582-9

Zhang, T. C., Zou, Q. L., Jia, X. Q., Jiang, C. Z., and Niu, X. G. (2022). Effect of SiO2 nanofluid with different concentrations on the wettability of coal. *Fuel* 321, 124041. doi:10.1016/j.fuel.2022.124041

Zhao, J. J., Tian, S. X., Li, P., Xie, H. G., and Cai, J. J. (2023a). Molecular dynamics simulation and experimental research on the influence of SiO2-H2O nanofluids on wettability of low-rank coal. *Colloids Surfaces A Physicochem. Eng. Aspects* 679, 132580. doi:10.1016/j.colsurfa.2023.132580

Zhao, J. J., Tian, S. X., Xie, H. G., and Zhang, X. (2023b). Study of time-varying laws of stability and wettability of SiO2–H2O nanofluids with different particle sizes. *Industrial Eng. Chem. Res.* 62, 13529–13540. doi:10.1021/acs.iecr.3c02110

Zhao, Y. S., Feng, Z. C., and Chang, Z. X. (2003). Least energy priciple of dynamical failure of rock mass. *Chin. J. Rock Mech. Eng.* 11, 1781–1783.

Zou, D. Y., and Jiang, F. X. (2004). Research of energy storing and gestation mechanism and forecasting of rockburst in the coal and rock mass. *J. China Coal Soc.* 29 (2), 159–163.

Zou, Q. L., Chen, Z. H., Cheng, Z. H., Liang, Y. P., Xu, W. J., Wen, P. R., et al. (2022a). Evaluation and intelligent deployment of coal and coalbed methane coupling coordinated exploitation based on Bayesian network and cuckoo search. *Int. J. Min. Sci. Technol.* 32 (6), 1315–1328. doi:10.1016/j.ijmst.2022.11.002

Zou, Q. L., Ning, Y. H., Zhang, B. C., Tian, S. X., Jiang, Z. B., and An, Y. Q. (2023). Mechanical properties and failure characteristics of sandstone under ramp loading paths. *Geomechanics Geophys. Geo-Energy Geo-Resources* 9 (1), 39. doi:10.1007/s40948-023-00574-8

Zou, Q. L., Zhang, T. C., Ma, T. F., Tian, S. X., Jia, X. Q., and Jiang, Z. B. (2022b). Effect of water-based SiO2 nanofluid on surface wettability of raw coal. *Energy* 254, 124228. doi:10.1016/j.energy.2022.124228